Journal of Diabetes Science and Technology
Volume 3, Issue 4, July 2009

ORIGINAL ARTICLES

Enhanced Glucose Sensor Linearity Using Poly(Vinyl Alcohol) Hydrogels

SanthiSagar Vaddiraju, M.S.,[1] Hardeep Singh,[1] Diane J. Burgess, Ph.D.,[2]
Faquir C. Jain, Ph.D.,[3] and Fotios Papadimitrakopoulos, Ph.D.[1,4]

Abstract

Background:
High linearities, sensitivities, and low oxygen dependence constitute prime requisites for electrochemical glucose sensors. However, for implantable sensors the need to control tissue inflammation requires the use of outer membranes that permit inward analyte diffusion while continuously releasing anti-inflammatory drugs and other tissue response-modifying (TRM) agents. We have shown previously that while outer membranes based on layer-by-layer (LBL) assembly enhance linearity, poly(vinyl alcohol)(PVA) hydrogels loaded with TRM-containing microspheres enable a significant reduction in tissue inflammation. This article discusses the amperometric performance of glucose sensors coated with stacked LBL/PVA hydrogel outer membranes.

Methods:
Sensors were fabricated by immobilizing glucose oxidase enzyme on a 50-μm platinum wire followed by deposition of stacked LBL/PVA hydrogel outer membranes. The sensor response to various glucose concentrations was determined by applying 0.7 V vs an Ag/AgCl reference electrode in phosphate-buffered saline (37°C). Michaelis–Menten analysis was performed to quantify sensor performance in terms of linearity ($K^{app}_{m,glu}$) and oxygen dependence (K^{app}_{m,O_2}/[Glucose]).

Results:
When overlaid onto LBL-assembled outer membranes, PVA hydrogels improved sensor linearity by 60% from 10 to 16 m*M* of glucose and resulted in a twofold decrease in oxygen dependence.

Conclusions:
Enhancement in the performance of a PVA-coated sensor is attributed to the oxygen-storing capability of PVA hydrogel due to the formation of hydrophobic domains during its freezing and thawing employed to physical cross-link the PVA. Such membranes with the capability to release TRMs continuously while storing oxygen constitute a major improvement over current outer membrane technologies.

J Diabetes Sci Technol 2009;3(4):863-874

Author Affiliations: [1]Nanomaterials Optoelectronics Laboratory, Polymer Program, Institute of Materials Science, University of Connecticut, Storrs, Connecticut; [2]Department of Pharmaceutical Sciences, University of Connecticut, Storrs, Connecticut; [3]Nanomaterials Optoelectronics Laboratory, Electrical and Computer Engineering, University of Connecticut, Storrs, Connecticut; and [4]Department of Chemistry, University of Connecticut, Storrs, Connecticut

Abbreviations: (FAD) flavin adenine dinucleotide, (FT) freeze–thaw, (GO_x) glucose oxidase, (HA) humic acid, (LBL) layer by layer, (LRS) linear range sensitivity, (PBS) phosphate-buffered saline, (PPD) *ortho*-phenylenediamine, (PSS) poly(sodium 4-styrenesulfonate), (Pt) platinum, (PVA) poly(vinyl alcohol)

Keywords: apparent Michaelis-Menten constants, biosensor, freeze-thaw cycle, layer-by-layer assembly, linearity, outer membranes, oxygen content, oxygen dependence of biosensors, PVA hydrogels

Corresponding Author: Dr. Fotios Papadimitrakopoulos, Professor of Chemistry, Polymer Program, Institute of Material Science, U-3136, University of Connecticut, Storrs, CT 06269; email address papadim@mail.ims.uconn.edu

Introduction

The development of implantable biosensors for the continuous monitoring of glucose represents a critical step toward the development of an artificial pancreas. Device simplicity and analyte specificity of Clark-type electrochemical glucose sensors have been the primary reasons for their wide use in a range of applications.[1] First-generation Clark-type glucose sensors employ the flavoenzyme glucose oxidase (GO_x) immobilized on top of a working electrode.[1] The flavin adenine dinucleotide (FAD) redox cofactor of GO_x catalyzes the oxidation of glucose to glucorolactone, as shown in **Equations (1)** and **(2)**.

$$\text{Glucose} + GO_x(FAD) \rightarrow \text{Glucorolactone} + GO_x(FADH_2) \quad (1)$$

$$GO_x(FADH_2) + O_2 \rightarrow GO_x(FAD) + H_2O_2 \quad (2)$$

The generated H_2O_2 is assessed amperometrically on the surface of the working electrode via **Equation (3)**, which relates current to glucose concentrations as shown in **Figure 1**.

$$H_2O_2 \xrightarrow{V} O_2 + 2H^+ + 2e^- \quad (3)$$

In the case of subcutaneously implanted devices, the 1 to 2 orders of magnitude lower oxygen vs glucose concentration, over the normal to hyperglycemic range, present a major problem as there is insufficient oxygen to drive the reaction [**Equations (1)** and **(2)**], which eventually leads to signal saturation.[2] Following device implantation, this is further compounded by inflammation, biofouling, and fibrotic encapsulation, which lead to additional variations in glucose-to-oxygen ratios.[1–6] While a number of semipermeable membranes have been developed to optimize the glucose-to-oxygen ratio,[7–18] only a few systems have been used with drug-releasing hydrogels,[17,18] designed to suppress inflammation, biofouling, and fibrotic encapsulation. The typical approach to counter both these issues is the use of overlaid membranes in which the inner membrane limits glucose diffusion and the outer membrane counters fibrotic encapsulation.[19,20] Such dual membrane systems, however, come at the expense of increasing response time and decreasing sensitivity.[19]

In order to reduce membrane thickness and fine-tune permeability, we have employed layer-by-layer (LBL) assemblies based on charged polymers and/or multivalent cations (i.e., Fe^{3+}).[7,11,12,21] In particular, the combination of five humic acid (HA)/Fe^{3+} bilayers has been shown to enhance linearity while at the same time reducing sensor response time through the facile outer diffusion of H_2O_2.[21] In a separate development, our group has shown that poly(vinyl alcohol) (PVA) hydrogels containing dexamethasone-loaded poly(lactic-*co*-glycolic acid) microspheres are capable of suppressing inflammation in excess of 1 month.[11,22–26] Unlike other systems that use reactive cross-linking agents,[19,20,27] both LBL and PVA hydrogels rely on physical cross-linking based on ionic interactions[7,11,12,21,28] and freeze–thaw (FT)-induced phase separation,[22,29,30] respectively, which eliminates the possibility of side reactions with the underlying enzyme layer. The number of freeze–thaw cycles has been shown to exert a strong influence on these hydrogels, controlling both the modulus and the degree of hydration.[22,29] These macroscopic physical attributes of PVA are expected to influence its permeability for glucose and O_2 and, as a consequence, device performance, thereby necessitating a separate investigation of PVA-coated glucose sensors.

With this in mind, we have investigated the performance of glucose sensors coated with stacked LBL/PVA hydrogel membranes as a function of LBL microstructure and the extent of PVA hydrogel FT cycling. It was determined that the PVA hydrogels not only allow for a facile diffusion of glucose and oxygen, but also store oxygen effectively, which is intimately dependent on the number of FT cycles. Consequently, introduction of a PVA hydrogel coating resulted in increased sensor linearity, while registering a significantly lower decrease in sensor sensitivity compared to other stacked membrane systems.[19,20] More interestingly, sensor performance is controlled solely by the diffusion characteristics of the inner membrane, while the outer PVA hydrogel supplements the sensor oxygen levels. The oxygen-absorbing property of the PVA hydrogel is related to the amount of hydrophobic physically cross-linked domains within the hydrogel, which is directly proportional to the number of FT cycles. Such dual membranes offer significant advantages over presently available outer membranes in lieu of their ability to control tissue reactions through the controlled release of TRMs, while allowing inner diffusion of analytes and supplemental storage of oxygen.

Materials and Methods

Glucose oxidase enzyme (E.C. 1.1.3.4, 157,500 units/g, *Aspergillus niger*), glutaraldehyde [25(w/v)% solution in water], *ortho*-phenylenediamine (PPD), bovine serum albumin, sodium salt of HA (molecular mass 169 kDa), ferric chloride hexahydrate (reagent grade), D-glucose (reagent grade), poly(sodium 4-styrenesulfonate)(PSS)

(M_w 70,000), and poly(diallyldimethylammonium chloride) (PDDA)[20(wt)% in water; M_w 200,000–350,000] were purchased from Sigma. PVA (99% hydrolyzed, molecular mass 133 kDa) was obtained from Polysciences Inc. (Warrington, PA). The platinum (Pt) and silver wires were purchased from Ladd Research.

The fabrication of working electrodes was achieved as described previously.[21]

The LBL assembly of semipermeable membranes was performed as described elsewhere.[21] In brief, this was achieved by dipping the GO_x-covered working electrodes alternately in solutions of HA or PSS and $FeCl_3 \cdot 6H_2O$ or PDDA to yield devices A_5 (HA/Fe^{3+}), B_5 (HA/PDDA), and C_5 (PSS/PDDA).

For the preparation of PVA solutions, 10% (w/v) aqueous solutions of 99% hydrolyzed PVA were preheated to ca. 80°C to facilitate complete polymer dissolution.

For deposition of LBL/PVA hydrogel-stacked membranes, following LBL assembly, devices A_5, B_5, and C_5 were coated by dip coating the working electrode in the as prepared PVA solution and were immediately gelled by freezing at –20°C for 2 hours, followed by thawing for 1 hour at room temperature. Subsequently, a number of freeze–thaw cycles (N) were performed, with the total N varying between 1 and 7. Depending on the type of LBL device (A_5, B_5, or C_5), the stacked devices were denoted as A_5P_N, B_5P_N, or C_5P_N, respectively. It is worth noting here that since surface defects such as cracks and exposed edges in PVA change its analyte diffusion rates, care was taken during dip coating to ensure (1) no cracks, exposed edges, and complete coverage by utilizing an 18-gauge needle-based mold and (2) no trapped air bubbles (by applying low vacuum) in the PVA hydrogel, which generally lead to holes and cracks during FT cycling of the PVA hydrogel.

Degree of swelling of PVA (water uptake) experiments were performed in phosphate-buffered saline (PBS) buffer at room temperature. Air-dried PVA samples with an initial mass of M_0 were weighed and immersed in 20 ml of PBS buffer. At regular time intervals (t), excess fluid from swollen samples was carefully wicked away and the weight change ($M_t - M_0$) was recorded. The percent weight change was defined as $(M_t - M_0)/M_0 \times 100\%$. This experiment was repeated as a function of FT cycling. The oxygen content of the PVA hydrogels was used to confirm its oxygen-storing capability as a result of formation of water-free hydrophobic domains that act as physical cross-links. This was achieved by sealing a known amount of dried PVA sample in a glass tube under vacuum. The PVA hydrogel sample was gelled via FT cycling and dried in a desiccator (until no significant weight loss was observed) prior to flame sealing the tube under vacuum to ensure an oxygen-free environment in the sealed glass tube. This hydrogel-containing sealed glass tube was then placed in an air-tight chamber containing 50 ml of deionized water and a commercial oxygen sensor (Mettler Toledo, Model 4100e). Following this step, the test cell was sealed from the atmosphere and N_2 was bubbled in to remove the oxygen in the test cell. When the oxygen concentration in the test cell reached 0 μM (ca. 20 minutes), the PVA hydrogel-containing glass tube was then crushed to let its oxygen level equilibrate with the surrounding media. The increase in the oxygen level was recorded as a function of the number of FT cycles, and the experiment was repeated in triplicate.

In vitro amperometric experiments were performed as described previously.[21] A 3-hour induction period was allowed in order to attain complete swelling of the PVA hydrogel (see **Figure A1A** in the Appendix) before commencement of the amperometric experiments.

For determination of apparent Michaelis–Menten constants for glucose ($K^{app}_{m,glu}$) and oxygen (K^{app}_{m,O_2}), along with the linear range sensitivity (LRS) of the sensor, analysis was performed as described elsewhere,[21] using **Equation (4)**:

$$J_{glu} = \frac{J_{max}}{\frac{K^{app}_{m,O_2}}{[O_2]} + \frac{K^{app}_{m,glu}}{[Glu]}}, \quad (4)$$

where J_{glu} is the amperometric current density (Amp/cm^2) for a particular concentration of glucose ([Glu]) and oxygen ([O_2]) and J_{max} is the saturation response J_{glu}. In brief, the amperometric response of the sensor at various glucose concentrations or various oxygen concentration was fitted into the Michaelis–Menten equation shown in **Equation (4)** to yield $K^{app}_{m,glu}$ or K^{app}_{m,O_2}, respectively. The LRS of these sensors, which is the initial slope of J_{glu} vs glucose concentration, is determined, as described elsewhere, using **Equation (5)**:[31]

$$LRS = \frac{J_{max}}{K^{app}_{m,glu}}. \quad (5)$$

Statistical analysis

At least three sensors of each kind were fabricated and tested. Values of J_{glu} and K^{app}_{m,O_2} were plotted as the mean obtained from three sensors of a similar kind. The LRS, $K^{app}_{m,glu}$, and slope of K^{app}_{m,O_2} vs oxygen concentration (K^{app}_{m,O_2}[Glu]) are presented as the mean ± standard deviation, obtained from three sensors of a similar kind. It is worth mentioning here that the error for a single sensor tested thrice is close to zero and is negligible.

Results

Figure 1 is a schematic of the cross section of the working electrode for the devices under investigation. The Pt working electrode was coated with a thin (ca. 10 nm) electropolymerized PPD layer in order to block the oxidation of other endogenous species such as ascorbic acid, uric acid, and acetaminophen, which are likely to oxidize at the operating potential of the sensor (selectivity of up to 95% was obtained compared to a bare Pt working electrode, data not shown).[9,32,33] The GO_x enzyme was subsequently immobilized by dip coating the Pt/PPD electrode in a solution of GO_x followed by cross-linking with glutaraldehyde. In order to regulate the inward diffusion of glucose, the GO_x-coated, Pt-working electrodes were then coated with five bilayers of HA/Fe^{3+} (device A_5), HA/PDDA (device B_5), or PSS/PDDA (device C_5) via LBL assembly. Devices employing stacked LBL/PVA hydrogel membranes were realized by dip coating the LBL membrane-covered working electrode in a PVA solution, followed by repetitive FT cycles to yield devices A_5P_N, B_5P_N, or C_5P_N, where N is the number of FT cycles. It has been well established that FT cycling of aqueous PVA solutions causes water microcrystallization, which in turn causes partial PVA dehydration.[22,29] These water-poor PVA domains self-order into hydrophobic structures and, unless heated to high temperatures (ca. 50–80°C), they remain insoluble in water, thereby acting as physical cross-links.[29] The higher the number of FT cycles, the larger and more ordered these hydrophobic structures become. Galeska and colleagues[22] have shown that the modulus of the hydrated PVA hydrogels increases by an order of magnitude from one to five FT cycles to reach a shear modulus value comparable to that of human tissue.[22,34] **Figure A1A** in the **Appendix** illustrates the uptake of water as a function of the number of FT cycles and the immersion time in PBS buffer solution. Typically these hydrogels reach saturation swelling at ca. 3 hours at room temperature (25°C), while equilibrium is attained in less than 20 minutes at 37°C from the dried state.[22] In addition, saturation swelling decreases steadily by ca. 26% every two FT cycles from 350% for one FT cycle down to 140% for seven FT cycles with minute signs of saturation at higher FT cycles (**Figure A1B** in the **Appendix**).

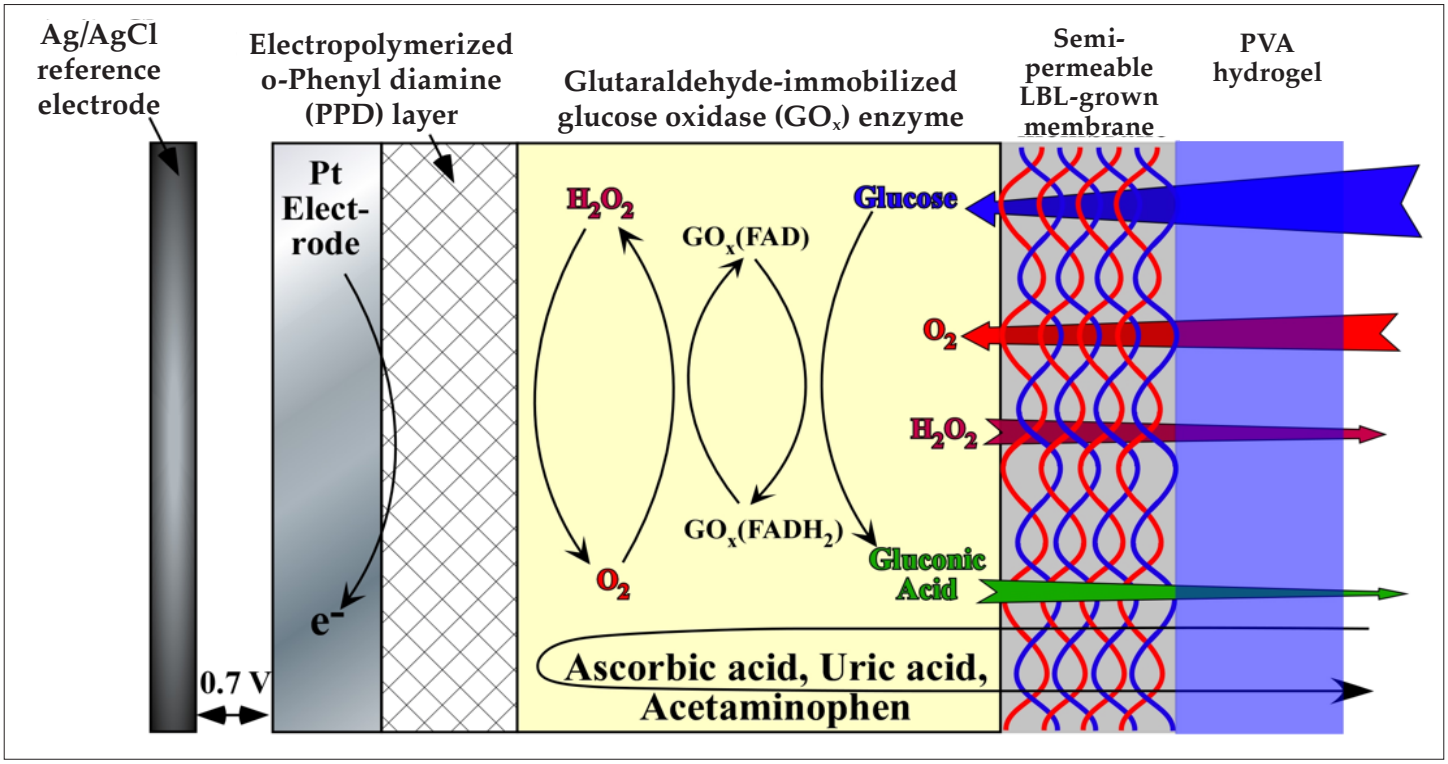

Figure 1. Schematic cross section of the glucose sensor in study.

Figure 2 illustrates the response of devices A_5, B_5, and C_5 before and after the addition of a PVA hydrogel (cross-linked by three FT cycles) as a function of glucose concentration. The response of these sensors in the physiologically significant glucose range, as well as the response of the sensors with no outer membrane, is shown in **Figures A2** and **A3** in the **Appendix**, respectively. For all sensors, the addition of glucose resulted in an increase and eventual saturation of their amperometric response at high glucose concentrations. It is worth mentioning that the physiological glucose concentration range (including hypo- and hyperglycemic minimum and maximum) is within the hatched box spanning between 2 and 22 m*M* of glucose, respectively (**Figure 2**). The addition of five bilayers of LBL membranes lowered the saturation amperometric response by ca. 60, 25, and 15% for devices A_5, B_5, and C_5, respectively, as obtained from **Figures 2** and **A3**. Similarly, addition of the PVA hydrogel lowered the saturation amperometric response by ca. 50, 30, and 15% for devices A_5P_3, B_5P_3, and C_5P_3, respectively.

Table 1 illustrates the Michaelis–Menten constant for glucose ($K^{app}_{m,glu}$), linear range sensitivity, and oxygen slope (K^{app}_{m,O_2}/[Glu]) for all sensors shown in **Figure 2**. The addition of five bilayers of LBL membranes (device A_5, B_5, and C_5) onto the control sensor (with no outer membrane) showed a 25 to 350% increase in $K^{app}_{m,glu}$ and a 25 to 90% decrease in LRS as compared to control sensors. The trends in LRS and $K^{app}_{m,glu}$ among these LBL-coated sensors are in agreement with previously reported results.[21] The incorporation of three FT-cycled PVA layers on top of the LBL membranes (devices A_5P_3, B_5P_3, and C_5P_3) resulted in a 40 to 75% increase in $K^{app}_{m,glu}$ and a 50% decrease in sensitivity. The trends in LRS and $K^{app}_{m,glu}$ for devices A_5P_3, B_5P_3, and C_5P_3 are similar to

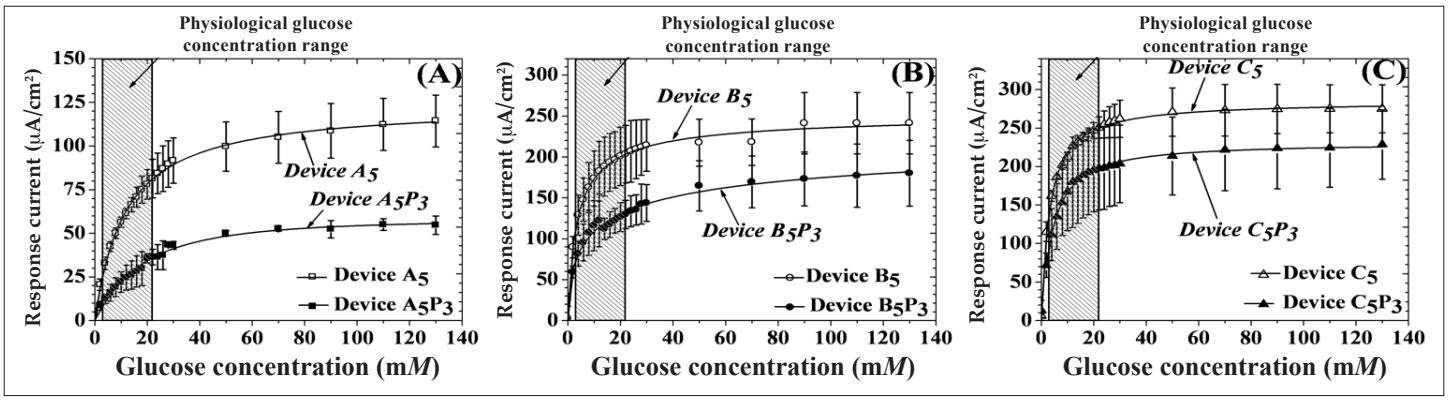

Figure 2. Saturation amperometric current vs glucose concentration for sensors containing five bilayers of (**A**) HA/Fe^{3+}, (**B**) HA/PDDA, and (**C**) PSS/PDDA semipermeable membranes, before and after deposition of PVA hydrogels, subjected to three freeze–thaw cycles. Hatched regions illustrate the observed physiological glucose concentration.

Table 1.
Performance Criteria of Various Sensors Containing Different Outer Semipermeable Membranes

Type of LBL membrane	Before PVA				After PVA			
	Sensor name	$K^{app}_{m,glu}$ [a]	LRS [b]	Oxygen slope [c]	Sensor name	$K^{app}_{m,glu}$ [a]	LRS [b]	Oxygen slope [c]
HA/Fe^{3+}	A_5	11 ± 2	11.0 ± 0.4	9.0 ± 1	A_5P_3	14 ± 4	4 ± 1	5 ± 1
HA/PDDA	B_5	3.3 ± 0.3	7 × 10^1 ± 1 × 10^1	23 ± 8	B_5P_3	4 ± 0.4	4 × 10^1 ± 2 × 10^1	19 ± 3
PSS/PDDA	C_5	3 ± 1	10 × 10^1 ± 3 × 10^1	23 ± 3	C_5P_3	4 ± 2	5.6 × 10^1 ± 2 × 10^1	20 ± 3
None	Control	2.3 ± 0.3	13 × 10^1 ± 4 × 10^1	29 ± 5				

[a] Michaelis–Menten constant ($K^{app}_{m,glu}$)(in m*M* of glucose).
[b] Linear range sensitivity (in μAcm^{-2}m*M*$^{-1}$).
[c] Initial O_2 slope (K^{app}_{m,O_2}/[glucose])(in μMO_2 mM^{-1}Glu).

devices A_5, B_5, and C_5, wherein device A_5P_3 displayed a threefold higher $K^{app}_{m,glu}$ and an order of magnitude lower LRS than devices B_5P_3 and C_5P_3. The uniform decrease in device LRS by the incorporation of PVA signifies the fact that glucose flux toward the GO_x enzyme, and thereby the particular sensor performance, is controlled by the microstructure of the LBL membrane.[21]

In order to obtain a more complete picture of the influence of oxygen in these sensors, the K^{app}_{m,O_2} values were also determined for the sensors in **Figure 2**. **Figure 3** depicts the K^{app}_{m,O_2} of all aforementioned sensors as a function of glucose concentration within the physiological observed regime. The K^{app}_{m,O_2} of the control sensor with no outer membrane is shown in **Figure A4** in the **Appendix**. The K^{app}_{m,O_2} of all these sensors tend to saturate at higher glucose concentrations in accordance with earlier reports.[21] The addition of five bilayers of LBL membranes resulted in a 65, 9, and 5% decrease in the saturation K^{app}_{m,O_2} values for devices A_5, B_5, and C_5, respectively, as obtained from **Figures 3** and **A3**. The addition of a PVA hydrogel lowered the saturation K^{app}_{m,O_2} values by ca. 35, 12, and 6% for devices A_5P_3, B_5P_3, and C_5P_3, respectively. In accordance with the relative increase in $K^{app}_{m,glu}$ values of each of the three sensors when PVA was incorporated, the K^{app}_{m,O_2} values, at all glucose concentrations tested, decreased proportionally.

The slope of the K^{app}_{m,O_2} vs glucose concentration curves (i.e., K^{app}_{m,O_2}[Glu]) at low glucose concentrations provides a more comprehensive picture of the oxygen dependence of these sensors (**Table 1**). The larger the slope, the more depleted these sensors of oxygen are.[21,35] The 20 to 70% decrease in K^{app}_{m,O_2}[Glu] upon the incorporation of five bilayers of LBL membranes is further reduced by 15 to 45% by the additional PVA layer.

In order to elucidate the effect of the cross-link density of PVA on the performance of the device, we selected the five bilayer LBL-assembled HA/Fe^{3+}-coated sensor (device A_5) and varied the number of PVA freeze–thaw cycles. **Figure 4A** displays the variation of $K^{app}_{m,glu}$ and J_{max} as a function of FT cycles for devices A_5P_N, where N ranges from 1 to 7.

These data have been obtained from the corresponding amperometric response vs glucose concentration curves of **Figures 2A** and **A5**. The $K^{app}_{m,glu}$ displayed an initial increase at two FT cycles that was followed by a gradual decrease and saturation at higher FT cycles. However, the J_{max} of these devices shows a steady increase until three FT cycles followed by a steady decrease at higher FT cycles. **Figure 4B** shows the corresponding variation in the initial oxygen slope of these devices according to the number of FT cycles. These data have been obtained from the corresponding K^{app}_{m,O_2} vs glucose concentration curves of **Figures 3A** and **A6**. In accordance with the $K^{app}_{m,glu}$ values, the initial oxygen slope of these sensors displayed a minimum at two to three FT cycles before starting to increase and potentially saturating at higher FT cycles.

The well-known feature of PVA to form water-free hydrophobic domains that act as physical cross-links prompted an investigation of its oxygen-storing capability as a function of FT cycles. For this, following application of the desired FT cycles, a known amount of PVA was sealed in a glass tube and crushed to release the specimen in an oxygen-free environment to measure its equilibrated oxygen content. **Figure 5** illustrates the variation of stored oxygen (in parts per million of O_2 per dry PVA) as a function of FT cycles. The degree of oxygen storage of PVA increased linearly with an increasing number of FT cycles. PVA

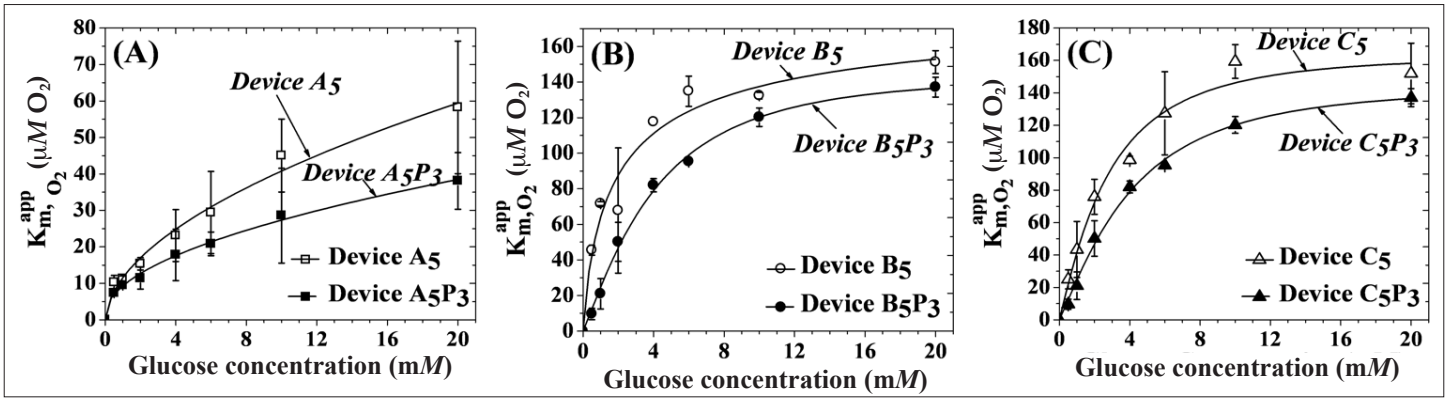

Figure 3. Variation of K^{app}_{m,O_2} as a function of glucose concentration for sensors containing five bilayers of (**A**) HA/Fe^{3+}, (**B**) HA/PDDA, and (**C**) PSS/PDDA semipermeable membranes, before and after deposition of PVA hydrogels, subjected to three freeze–thaw cycles. The slope of each curve below 4 mM of glucose allowed determination of the K^{app}_{m,O_2}[*Glu*] term, which is inversely proportional to the amount of oxygen within the sensor.

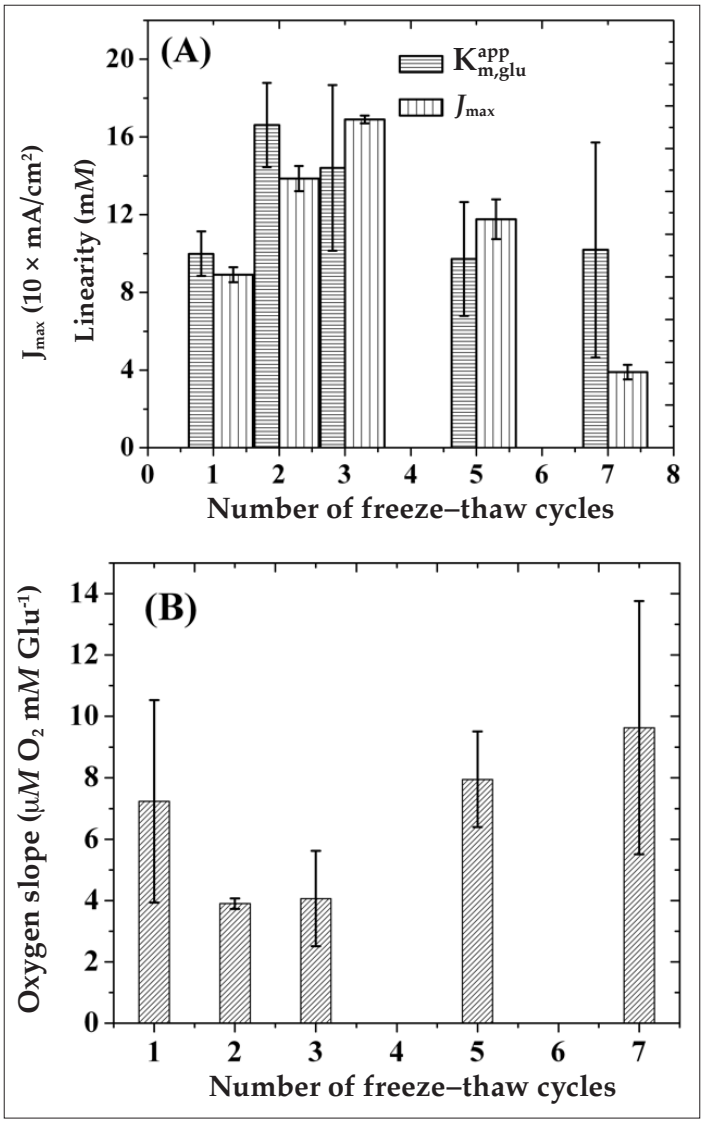

Figure 4. Variation of (**A**) sensor linearity ($K^{app}_{m,glu}$) and LRS and (**B**) oxygen slope (K^{app}_{m,O_2}[Glu]) as a function of the number of freeze–thaw cycles for sensors coated with (HA/Fe^{3+})^5/PVA hydrogel outer membranes.

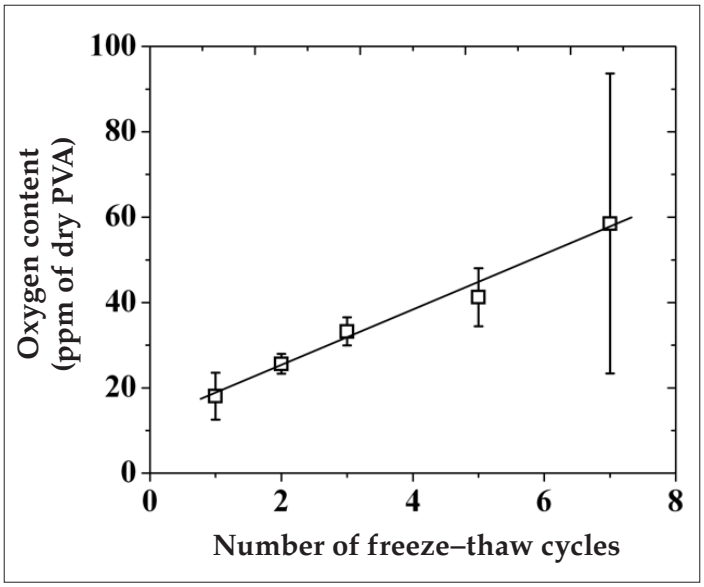

Figure 5. Variation of the oxygen content [parts per million (ppm) of O_2 per dry PVA] of PVA hydrogel as a function of the number of freeze–thaw cycles.

hydrogels subjected to a 7 $N_{F/T}$ cycle displayed a threefold higher oxygen content than that of hydrogels subjected to 1 $N_{F/T}$ cycles. In addition, the trend in the variation of oxygen content of PVA as a function of the number of FT cycles is in inverse relation to the trend in the saturation swelling of PVA (**Figure A1B** in the **Appendix**).

Discussion

Over the years a number of diffusion-limiting outer membranes that enhance the performance of an implantable glucose sensor have been reported.[7–20] However, only a few of these membranes are capable of simultaneously reducing the large glucose/O_2 ratio and releasing tissue response modifiers that suppress inflammation and fibrotic encapsulation. With this in mind, a stacked configuration of outer membranes based on ultrathin LBL-assembled films and PVA hydrogels are currently shown to provide a powerful combination to regulate glucose with the inner membrane and improve its ratio with O_2, while the outer PVA hydrogel layer can be loaded with drug-releasing microspheres capable of suppressing inflammation in excess of 1 month.[11,22–26] Apart from this drug-releasing ability, PVA hydrogels afford versatile cross-linking via freeze–thaw cycling that alleviates the use of reactive cross-linking agents (which can lead to a number of unwanted side reactions)[30,36,37] while maintaining a modulus similar to that of human tissue. Moreover, the well-known permeability of three to five FT-cycled PVA hydrogels for glucose and proteins[38] renders any PVA-induced sensitivity loss minimal. This article demonstrated that the PVA layer possesses another useful attribute to the sensor, which stems from its O_2-storing capability. This was illustrated by the enhancement in sensor linearity (**Table 1**) and by direct experimental measurement of the O_2 content (**Figure 5**). In addition, sensor performance in terms of linearity and sensitivity was shown to peak at two to three FT cycles, which results in a modulus comparable to that of human tissue.[22]

The complex behavior of sensor performance (i.e., $K^{app}_{m,glu}$, LRS, and K^{app}_{m,O_2}/[Glu]) as a function of FT cycles (**Figure 4**) can be understood by taking into account two opposite trends. As shown in **Figure 5**, increasing the number of FT cycles increases the PVA oxygen content. However,

as the number of FT cycles increases, the PVA water uptake decreases (**Figure A1B** in the **Appendix**) and the modulus increases, thereby leading to a decrease in the hydrogel pore size, which subsequently suppresses analyte (glucose and O_2 cosubstrate) diffusivities. While the former enhances sensor sensitivity, the latter reduces it. These arguments qualitatively explain the initial (below two to three FT cycles) enhancement in sensor performance shown in **Figure 4A** (in terms of linearity and sensitivity) and **Figure 4B** (in terms of oxygen dependence), suggesting that storing more oxygen in the vicinity of the GO_x enzyme (i.e., PVA over layer) is as effective as storing it within the GO_x layer. For higher FT cycles, restriction in both glucose and oxygen diffusivity explains the gradual decay in sensor performance. In order for this to hold, the chemical potential for the inner diffusion of glucose must slightly outweigh that of O_2. This appears to contradict the expected diffusivities based on their relative size. However, upon closer inspection, the measured diffusivities through $(HA/Fe^{3+})_5$ membranes are not that different.[21] When the measured diffusivity ratio of glucose and oxygen through (HA/Fe^{3+}) (ca. 0.8) is compared with the reactivity ratio of GO_x(FAD) for glucose and of $GO_x(FADH_2)$ for oxygen (ca. 4),[39] it becomes apparent that the chemical potential that the oxygen experiences is about three to four times less than that of glucose (a molecule with a much larger size). This explains the need to actively store oxygen within the semipermeable membranes and not rely exclusively on size-dependent diffusivity differences of substrate and cosubstrate.

Conclusions

The performance of miniaturized implantable glucose sensors coated with stacked layer-by-layer and poly(vinyl alcohol) hydrogel outer membranes has been investigated. Such configuration provides effective analyte regulation together with the ability to immobilize various drug-releasing entities within the PVA hydrogel. It was further shown that the outer PVA hydrogel can store O_2, which improved sensor linearity by 60% to as high as 16 m*M* of glucose. An increase in the number of FT cycles was determined to increase the oxygen-storing capability of the PVA hydrogel due to the formation of larger hydrophobic domains, acting as physical cross-links. The interplay between sensor performance (in terms of linearity, sensitivity, and oxygen dependence) and oxygen storage was elucidated using various LBL membranes and FT cycles. LBL films based on five bilayers of humic acid/Fe^{3+}, along with three FT-cycled PVA hydrogels, were shown to provide the optimum performance along with a modulus that closely matches that of subcutaneous human tissue. Further fine-tuning of these two membranes is expected to extend sensor linearity beyond the currently reported 16 m*M* of glucose and more closer to the required 22 m*M* of glucose.

Acknowledgements:

Financial support for this study was obtained from U.S. Army Medical Research Grants (DAMD17-02-1-0713, W81XWH-04-1-0779, W81XWH-05-1-0539, and W81XWH-07-10668) and NIH/NHLBI 1-R21-HL090458-01.

References:

1. Wilson GS, Gifford R. Biosensors for real-time in vivo measurements. Biosens Bioelectron. 2005;20(12):2388-403.
2. Heller A. Implanted electrochemical glucose sensors for the management of diabetes. Annu Rev Biomed Eng. 1999;1:153-75.
3. Gerritsen M, Jansen JA, Lutterman JA. Performance of subcutaneously implanted glucose sensors for continuous monitoring. Neth J Med. 1999;54(4):167-79.
4. Koschinsky T, Heinemann L. Sensors for glucose monitoring: technical and clinical aspects. Diabetes Metab Res Rev. 2001;17(2):113-23.
5. Shichiri M, Yamasaki Y, Kawamori R, Hakui N, Abe H. Wearable artificial endocrine pancreas with needle-type glucose sensor. Lancet. 1982;2(8308):1129-31.
6. Wang J. Glucose biosensors: 40 years of advances and challenges. Electroanalysis. 2001;13(12):983-8.
7. Galeska I, Chattopadhyay D, Moussy F, Papadimitrakopoulos F. Calcification-resistant nafion/Fe^{3+} assemblies for implantable biosensors. Biomacromolecules. 2000;1(2):202-7.
8. Harrison DJ, Turner RF, Baltes HP. Characterization of perfluorosulfonic acid polymer coated enzyme electrodes and a miniaturized integrated potentiostat for glucose analysis in whole blood. Anal Chem. 1988;60(19):2002-7.
9. Moussy F, Harrison DJ, O'Brien DW, Rajotte RV. Performance of subcutaneously implanted needle-type glucose sensors employing a novel trilayer coating. Anal Chem. 1993;65(15):2072-7.
10. Praveen SS, Hanumantha R, Belovich JM, Davis BL. Novel hyaluronic acid coating for potential use in glucose sensor design. Diabetes Technol Ther. 2003;5(3):393-9.
11. Galeska I, Hickey T, Moussy F, Kreutzer D, Papadimitrakopoulos F. Characterization and biocompatibility studies of novel humic acids based films as membrane material for an implantable glucose sensor. Biomacromolecules. 2001;2(4):1249-55.
12. Tipnis R, Vaddiraju S, Jain F, Burgess D, Papadimitrakopoulos F. Layer-by-layer assembled semipermeable membrane for amperometric glucose sensors. J Diabetes Sci Technol. 2007;1(2):193-200.
13. Yang Y, Zhang SF, Kingston MA, Jones G, Wright G, Spencer SA. Glucose sensor with improved haemocompatibilty. Biosens Bioelectron. 2000;15(5-6):221-6.
14. Ishihara K, Tanaka S, Furukawa N, Kurita K, Nakabayashi N. Improved blood compatibility of segmented polyurethanes by polymeric additives having phospholipid polar groups. I. Molecular design of polymeric additives and their functions. J Biomed Mater Res. 1996;32(3):391-9.

15. Allen DJ, Johnson KW, Nevin RS. US patent 5322063; 1994.

16. Suri JT, Cordes DB, Cappuccio FE, Wessling RA, Singaram B. Continuous glucose sensing with a fluorescent thin-film hydrogel. Ang Chem Int Ed Engl. 2003;42(47):5857-9.

17. Wu Y, Rojas AP, Griffith GW, Skrzypchak AM, Lafayette N, Bartlett RH, Meyerhoff ME. Improving blood compatibility of intravascular oxygen sensors via catalytic decomposition of S-nitrosothiols to generate nitric oxide in situ. Sens Actuators. B Chem. 2007;121(1):36-46.

18. Gifford R, Batchelor MM, Lee Y, Gokulrangan G, Meyerhoff ME, Wilson GS. Mediation of in vivo glucose sensor inflammatory response via nitric oxide release. J Biomed Mater Res. 2005;75(4):755-66.

19. Yu B, Wang C, Ju YM, West L, Harmon J, Moussy Y, Moussy F. Use of hydrogel coating to improve the performance of implanted glucose sensors. Biosens Bioelectron. 2008;23(8):1278-84.

20. Wang C, Yu B, Knudsen B, Harmon J, Moussy F, Moussy Y. Synthesis and performance of novel hydrogels coatings for implantable glucose sensors. Biomacromolecules. 2008;9(2):561-7.

21. Vaddiraju S, Burgess DJ, Jain FC, Papadimitrakopoulos F. The role of H_2O_2 pt pt outer diffusion on the performance of implantable glucose sensors. Biosens Bioelectron. 2008:24(6):1557-62.

22. Galeska I, Kim TK, Patil SD, Bhardwaj U, Chatttopadhyay D, Papadimitrakopoulos F, Burgess DJ. Controlled release of dexamethasone from PLGA microspheres embedded within polyacid-containing PVA hydrogels. AAPS J. 2005;7(1):E231-40.

23. Hickey T, Kreutzer D, Burgess DJ, Moussy F. In vivo evaluation of a dexamethasone/PLGA microsphere system designed to suppress the inflammatory tissue response to implantable medical devices. J Biomed Mater Res. 2002;61(2):180-7.

24. Hickey T, Kreutzer D, Burgess DJ, Moussy F. Dexamethasone/PLGA microspheres for continuous delivery of an anti-inflammatory drug for implantable medical devices. Biomaterials. 2002;23(7):1649-56.

25. Patil SD, Papadimitrakopoulos F, Burgess DJ. Dexamethasone-loaded PLGA microspheres/PVA hydrogel composite coatings for inflammation control. Diabetes Technol Ther. 2004;6(6):887-97.

26. Bhardwaj U, Sura R, Papadimitrakopoulos F, Burgess DJ. Controlling acute inflammation with fast releasing dexamethasone-PLGA microsphere/PVA hydrogel composites for implantable devices. J Diabetes Sci Technol. 2006:1(1):8-17.

27. Guiseppi-Elie A, Brahim S, Slaughter G, Ward KR. Design of a subcutaneous implantable biochip for monitoring of glucose and lactate. IEEE Sensors. 2005;5(3):345-55.

28. Hammond PT, Whitesides GM. Formation of polymer microstructures by selective deposition of polyion multilayers using patterned self-assembled monolayers as template. Macromolecules. 1995;28:7569-71.

29. Hassan CM, Peppas NA. Structure and applications of poly(vinyl alcohol) hydrogels produced by conventional crosslinking or by freezing/thawing methods. Adv Poly Sci. 2000;153:37-65.

30. Azila AA, Barbari T, Searson P. Poly(vinyl alcohol): a potential matrix for glucose oxidase immobilization? Med J Malaysia. 2004;59 Suppl B:51-2.

31. McMahon CP, Killoran SJ, O'Neill RD. Design variations of a polymer-enzyme composite biosensor for glucose: enhanced analyte sensitivity without increased oxygen dependence. J Electroanal Chem. 2005;580:193-202.

32. McMahon CP, Killoran SJ, Kirwan SM, O'Neill RD. The selectivity of electrosynthesised polymer membranes depends on the electrode dimensions: implications for biosensor applications. Chem Commun (Camb). 2004;10(18):2128-30.

33. Kirwan SM, Rocchitta G, McMahon CP, Craig JD, Killoran SJ, O'Brien KB, Serra PA, Lowry JP, O'Neill RD. Modifications of poly(o-phenylenediamine) permselective layer on Pt-Ir for biosensor application in neurochemical monitoring. Sensors. 2007;7:420-37.

34. Yamada H. Strength of biological tissues. Baltimore (MD): Williams & Wilkins; 1970.

35. Dixon BM, Lowry JP, O'Neill RD. Characterization *in vitro* and in vivo of the oxygen dependence of an enzyme/polymer biosensor for monitoring brain glucose. J Neurosci Methods. 2002;119(2):135-42.

36. Wong FL, Abdul-Aziz A. Comparative study of poly(vinyl alcohol)-based support materials for the immobilization of glucose oxidase. J Chem Tech Biotech. 2008;83(1);41-6.

37. Doretti L, Ferrara D, Gattolin P, Lora S. Amperometric biosensor with physically immobilized glucose oxidase on a PVA cryogel membrane. Talanta. 1997;44(5):859-66.

38. Patil SD, Papadmitrakopoulos F, Burgess DJ. Concurrent delivery of dexamethasone and VEGF for localized inflammation control and angiogenesis. J Control Release. 2007;117(1):68-79.

39. Weibel MK, Bright HJ. The glucose oxidase mechanism. Interpretation of the pH dependence. J Biol Chem. 1971:246(9):2734-44.

Appendix

Degree of swelling of PVA films as a function of number of FT cycles

Figure A1A depicts the degree of swelling (water uptake) of PVA hydrogels in PBS buffer (pH 7.4) at room temperature as a function of immersion time for various FT cycles. Irrespective of the number of FT cycles, the water uptake increased with immersion time up to 3 hours before saturating at higher immersion times. Water uptake was inversely related to the number of freeze–thaw cycles, with hydrogels subjected to one FT cycle exhibiting a two- to threefold more water uptake than hydrogels with seven FT cycles. This differential water uptake can be related to the extent of physical cross-linking, which decreases porosity and alters fluid uptake.

Figure A1B depicts the saturation percent weight change of PVA hydrogels as a function of the number of freeze–thaw cycles, obtained from **Figure A1A**. The saturation swelling decreases steadily by ca. 26% every two FT cycles from 350% for one FT cycle down to 140% for seven FT cycles with minute signs of saturation at higher FT cycles. It is worth mentioning here that the trends in percent weight change of PVA hydrogels as a function of number of FT cycles (**Figure A1B**) are in inverse relation to trends in the oxygen content of PVA (**Figure 5**).

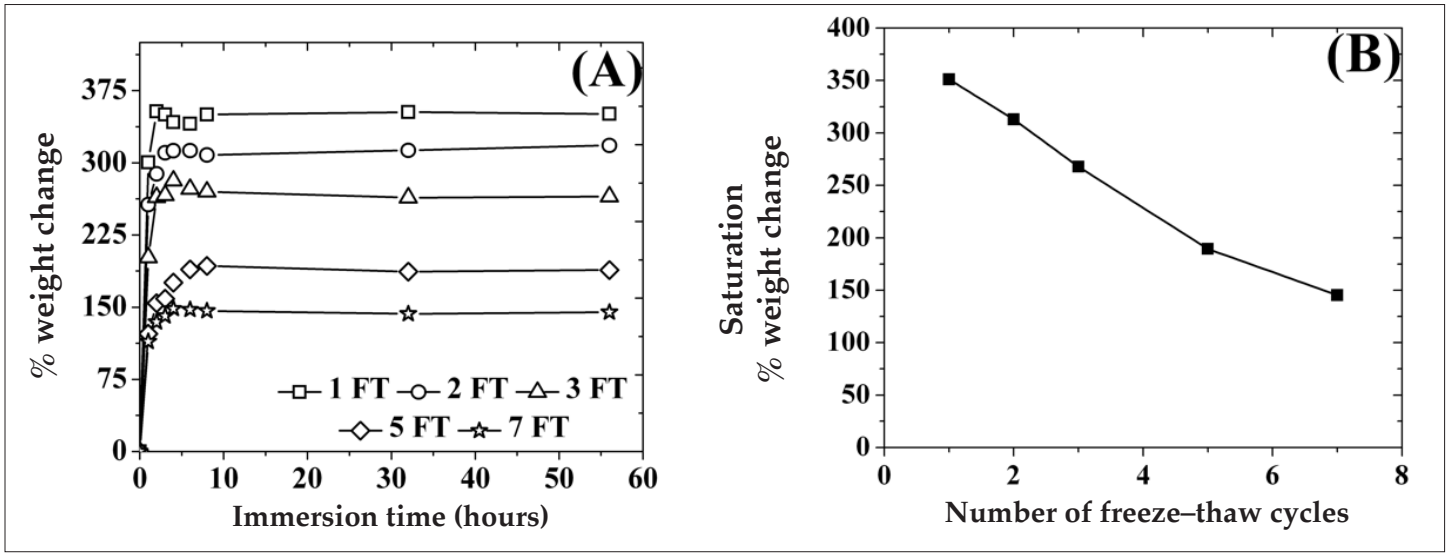

Figure A1. (**A**) Percent weight change of PVA hydrogels with various number of freeze–thaw cycles immersed in PBS buffer (pH 7.4) at room temperature as a function of the number of immersion time. (**B**) Saturation percent weight change of PVA hydrogels as a function of the number of freeze–thaw cycles.

Amperometric response of devices A_5, B_5, and C_5 before and after addition of PVA hydrogel within the physiologically significant glucose range

Figure A2 illustrates amperometric responses of the devices A_5, B_5, and C_5 before and after addition of a PVA hydrogel (cross-linked by three FT cycles) within the physiologically significant glucose range (2 to 22 m*M*). As can be seen, for all sensors, the addition of glucose resulted in an increase and eventual saturation of their amperometric response at glucose concentrations equal to their apparent Michaelis–Menten constant for glucose ($K^{app}_{m,glu}$)(**Table 1**).

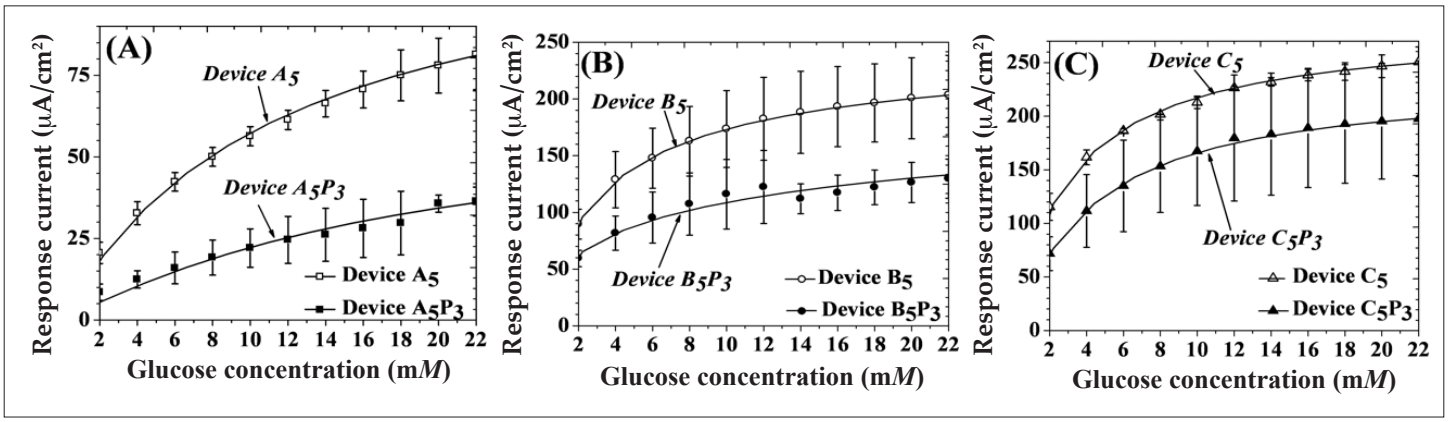

Figure A2. Saturation amperometric current vs glucose concentration (within the physiological glucose range) for sensors containing five bilayers of (**A**) HA/Fe^{3+}, (**B**) HA/PDDA, and (**C**) PSS/PDDA semipermeable membranes, before and after deposition of PVA hydrogels, subjected to three FT cycles.

Amperometric response of sensors with no outer membranes

Figure A3 shows the amperometric response of glucose with no outer membranes (Pt/PPD/GO_x) as a function of glucose concentration. As can be seen, the response of the sensor increased with increasing glucose concentration before saturating at higher glucose concentrations.

Oxygen dependence of sensors with no outer membranes

Figure A4 shows the plot of K_{m,O_2}^{app} as a function of glucose concentrations for devices with no outer membranes (Pt/PPD/GO_x).

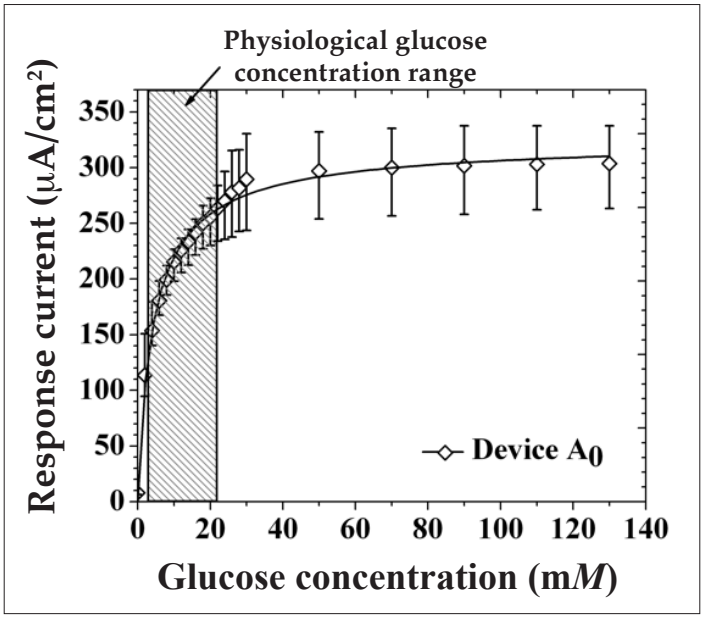

Figure A3. Saturation amperometric current vs glucose concentration for sensors with no outer membranes. The hatched region illustrates the observed physiological glucose concentration.

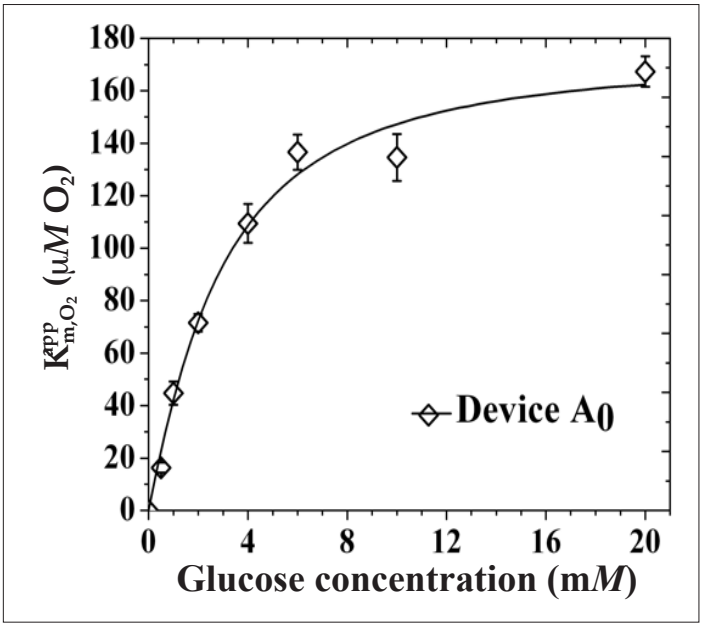

Figure A4. Variation of as a function of glucose concentration for sensors with no outer membranes.

Amperometric response of devices coated with five bilayers of HA/Fe^{3+} and PVA hydrogels (device A_5P_N) for various FT cycles of PVA

Figure A5 shows the amperometric response of devices A_5P_1, A_5P_2, A_5P_5, and A_5P_7 as a function of glucose concentration (the response of the A_5P_3 device is shown in **Figure 2A**). As before, the response of all the sensors increased with increasing glucose concentration before saturating at higher glucose concentrations.

Oxygen dependence of devices coated with five bilayers of HA/Fe^{3+} and PVA hydrogels (device A5PN) for various FT cycles of PVA

Figure A6 shows the plot of K^{app}_{m,O_2} as a function of glucose concentration devices A_5P_1, A_5P_2, A_5P_5, and A_5P_7 (the K^{app}_{m,O_2} of the A_5P_3 device is shown in **Figure 3A**). The slope of each curve below 4 m*M* of glucose allowed determination of the K^{app}_{m,O_2}/[Glu] term, which is inversely proportional to the amount of oxygen within the sensor.

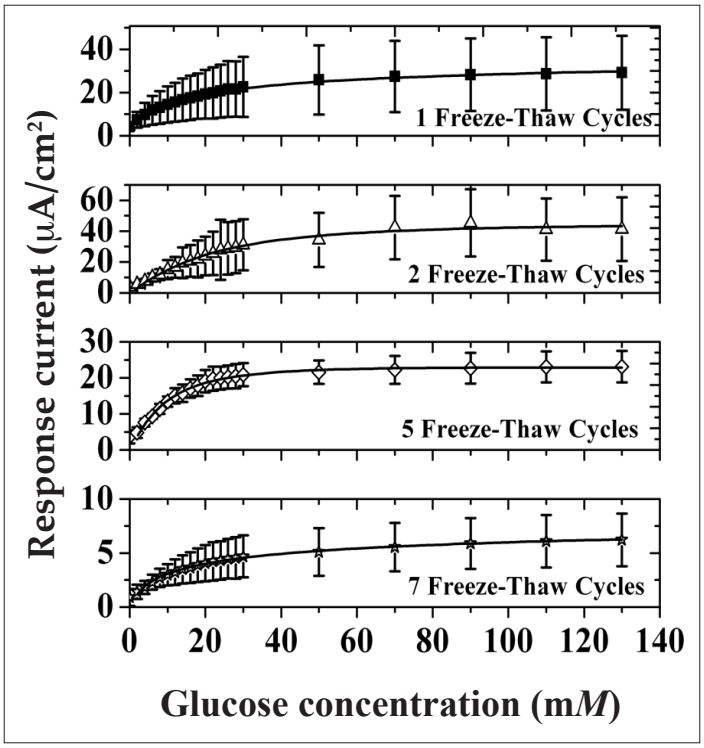

Figure A5. Saturation amperometric current vs glucose concentration for devices A_5P_1, A_5P_2, A_5P_5, and A_5P_7.

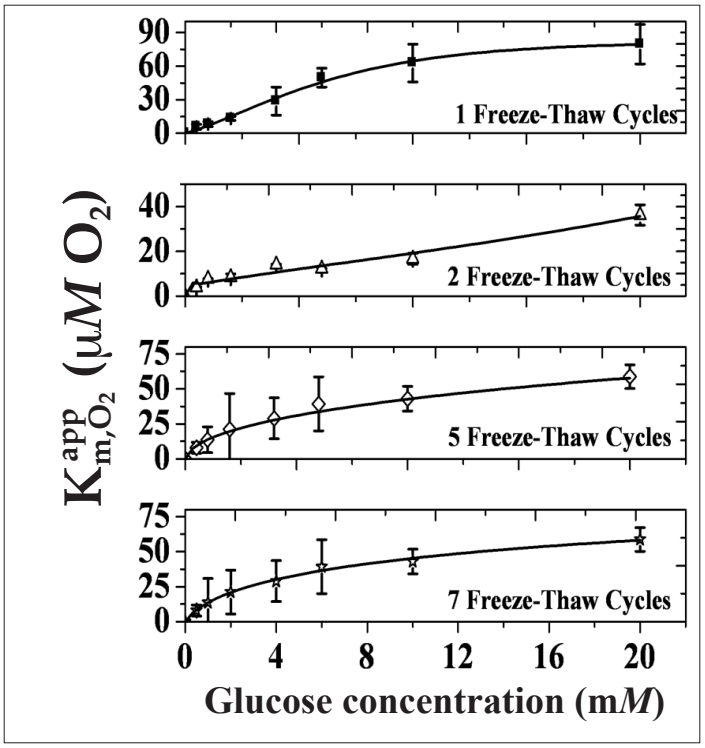

Figure A6. Variation of as a function of glucose concentration for devices A_5P_1, A_5P_2, A_5P_5, and A_5P_7.